PERGAMON

International Journal of Heat and Mass Transfer 42 (1999) 1059–1073

International Journal of HEAT and MASS TRANSFER

Role of inter- and intraparticle diffusion in nonuniform particle size gasless compacted-powder combustion synthesis—I: formulation

A. A. M. Oliveira, M. Kaviany*

Department of Mechanical Engineering and Applied Mechanics, The University of Michigan, Ann Arbor, MI 48109, U.S.A.

Received 20 December 1996; in final form 7 April 1998

Abstract

The propagation-mode, compacted-powder, gasless combustion synthesis of intermetallics is modeled through a combined three-scale, particle-level/specimen-level treatment. The specimen-level treatment is based on the local volume-averaged conservation equations for species and energy. The particle-level treatment considers a uniform temperature, the formation of products through a diffusion-controlled heterogeneous reaction, and allows for melting of the product assuming a distinct interface between the phases. The extent of conversion to the final product depends on the local availability of the reactants and through a statistical model and assuming that the interparticle mass transfer resistance is very large, it is determined a priori from the powder particle-size distribution. The influence of the particle-size distribution on the flame structure and the propagation speed is determined using the reaction rate of an average-size particle and also the ensemble average of the reaction rates experienced by particles of different sizes. In a follow-up article (Part II), the results of these models are compared with each other and with experimental results.

Nomenclature

A_{sa} specimen peripheral area [m^2]
c_p specific heat capacity [J kg^{-1} K^{-1}]
D diameter [m]
D_{A-C} binary diffusivity of species A [m^2 s^{-1}]
D_0 diffusion pre-exponential factor [m^2 s^{-1}]
f particle size distribution function
F fraction
h_{sa} heat transfer coefficient between specimen and ambient [W m^{-2} K^{-1}]
i specific enthalpy [J kg^{-1}]
$\langle k \rangle$ effective molecular thermal conductivity [W m^{-1} K^{-1}]
$\langle k_r \rangle$ effective radiant thermal conductivity [W m^{-1} K^{-1}]
l unit-cell characteristic length [m]
M molecular weight [kg kmol^{-1}]
$\dot{n}_{ls}$ volumetric melting rate [kg m^{-3} s^{-1}]
$\dot{n}_r$ volumetric reaction rate [kg m^{-3} s^{-1}]
N number of classes in the discrete particle size distribution function
r radial coordinate [m]
R radius [m]
R_g universal gas constant [J kmol^{-1} K^{-1}]
t time [s]
T temperature [K]
u velocity [m s^{-1}]
V volume of unit-cell [m^3]
V_s volume of specimen [m^3]
x axial coordinate [m]
Y mass fraction.

Greek symbols

$\Delta E_{a,D}$ diffusion activation energy [J kmol^{-1}]
Δi_r specific heat of combustion [J kg^{-1}]
Δi_{ls} specific heat of melting [J kg^{-1}]
Δi_m specific heat of mixing [J kg^{-1}]
ε porosity
v number of moles [kmol]
ρ density, mass concentration [kg m^{-3}].

* Corresponding author. Tel.: 001 734 936 0402; Fax: 001 734 647 3170; E-mail: kaviany@umich.edu

0017–9310/98/$—see front matter
PII: S0017–9310(98)00157–4

Subscripts
a ambient
ad adiabatic
A species A
B species B
c converted
C species C
e effective
f formation
F combustion front
g gas phase
i species *i*
l liquid-phase
m mixture
n nonreacted
r reaction, reacted, radiation or radial
s solid phase, specimen
sa between specimen and ambient
1 transformed coordinate.

Superscripts
A–C diffusion layer
0 standard state (pure component).

Other symbols
— ensemble average
$\langle\,\rangle$ local volume-averaged
$\langle\,\rangle i$ local phase-volume averaged.

1. Introduction

Combustion synthesis from compacted powders can be performed under the uniform (or explosion) mode or the propagation mode. In the propagation mode, the specimen is ignited at one end and a combustion wave travels through it converting the reactants to products. Here we consider the binary mixtures whose reactions are sufficiently exothermic such that the propagation occurs unaided (in contrast to the chemical-oven technique) and no substantial amount of gas is produced or participates in the reaction (i.e., gasless). Reviews on combustion synthesis are presented by Munir [1], Merzhanov [2], and Varma and Lebrat [3], among others. This method has been used to produce ceramics, intermetallics, cermets, and composites.

It has been observed experimentally that complete conversion may not occur and various intermediate phases may be formed [1–3]. Also, the maximum temperature in the combustion region may be substantially below the adiabatic equilibrium temperature. The lack of complete reaction is related to the heterogeneous nature of the polysize, multicomponent particle mixture (affecting the heat transfer, diffusion, and phase transformation), but the extent of the influence of the various mechanisms on the conversion to the final product, is not yet completely understood.

The modeling of combustion synthesis requires descriptions at the specimen and particle scales. At the specimen scale, the axial heat transfer, the volumetric heat generation, and the peripheral heat losses, determine the axial temperature distribution. The volumetric heat generation depends on the particle-level mass transfer, reaction rates, and phase transformations. The kinetic of these intraparticle processes depends on the temperature and chemical composition. The chemical composition is affected by species diffusion and by the interparticle availability of reactants. This local (i.e., interparticle) stoichiometry may differ from the specimen-level average stoichiometry because of the inherent heterogeneity of the medium which increases in the presence of a particle size distribution. The interaction between specimen-level and particle-level processes determines the final microstructure, including the composition and distribution of product phases and the amount of reactants remaining. The mechanical and morphological transformations during the combustion synthesis [e.g., the formation and destruction of porosity (i.e., consolidation), the mechanical stability of the compacts during reaction, and the products mechanical and metallographic properties] are not treated here. The modeling of these processes would require additional thermomechanical descriptions.

In previous modeling efforts, the specimen-level transport has been modeled using the local volume-averaged conservation equations and effective properties for energy and chemical species transport (i.e., macroscopic continuum models). The local thermal equilibrium hypothesis is used and the local chemical nonequilibrium results in product formation. The thermal effect of the chemical reactions is accounted for in the energy equation through the volumetric energy generation term (or through the total enthalpy if an enthalpy formulation is used). The volumetric reaction rate has been described either through a specimen-level kinetic model or through a particle-level diffusion model. In the specimen-level kinetic models, the particle-level reactions are either treated as homogeneous [4–7] or heterogeneous and diffusion limited [4, 8, 9]. In the particle-level diffusion models, a unit-cell model is developed and solved simultaneously with the specimen-level equations [10–18]. Phase change has been included in the heat of reaction [4], directly through the enthalpy form of the energy equation [6, 15], or using the phase-equilibrium conditions at the particle-level [17, 18]. The liquid phase has been assumed to wet the solid phase (wettability is related to chemical reactivity) and to redistribute locally, i.e., engulfing the solid particles [13–15].

At the particle-level, the differences between the various unit-cell models are related to the diffusion process and the route assumed for the formation of the final

product. The equilibrium[1] approach [17, 18] assumes that atomic interdiffusion of the initial elements occurs and the product formation follows phase-equilibrium conditions (i.e., phase diagram). The kinetics of phase nucleation is assumed sufficiently fast and all the phases present in the phase diagram are formed. If the required temperature is maintained and sufficient elapsed time is allowed, conversion to the specimen-level stoichiometric product is made. The nonequilibrium models assume simplified diffusion processes (which can be viewed as effective diffusion processes), and postulate the product formed [4, 10–15]. The unit-cell models allow for a more detailed account of the diffusion and for the inclusion of phase nucleation and transformation mechanisms and ultimately for a more complete treatment at the particle level. Another advantage of the unit-cell models is the ease of inclusion of particle size and particle-size distribution effects.

The effect of the powders particle-size distribution has not yet been analyzed in detail. Makino and Law [19] and Armstrong [12] have accounted for the effect of a bimodal particle-size distribution in the reaction rates. Aldushin et al. [20] considered the effect of the particle-size distribution assuming that the conversion to final product is complete (adiabatic equilibrium condition). They have shown that the nonuniform particle-size distribution does not affect appreciably the preheat region and the reaction front, but delays the complete conversion to the final product (because the diffusion in the larger grains requires longer elapsed times). The final stages of the combustion process is expected to be influenced by any heat losses, which then would enhance the effect of the particle-size distribution.

Here, a volume-averaged, specimen-level treatment along with a diffusion-reaction, nonequilibrium particle-level model is developed for binary systems. The model considers the formation of a single compound at the interface of the two reacting components. Local thermal equilibrium is assumed, the liquid phase is considered static, and the combustion front is assumed one-dimensional and propagating uniformly. Two mechanisms for the effects of the particle-size distribution are considered. First, since the chemical reaction is diffusion controlled, particles with different sizes experience different reaction rates and temperature evolution. This influences the specimen-level temperature distribution and propagation speed, as shown by Aldushin et al. [20]. The second mechanism is related to the local availability of the reactants. Due to the variation in particle size, it is possible to find regions that are rich in one of the reactants. Once, melted, the low melting-temperature reactant has the potential to spread over the other reactant particles. However, the distance separating the melt-rich regions from the melt-lean regions may be sufficiently large, thus preventing the timely migration of the melted reactant. In this case, total product conversion is not achieved, unless the liquid migration is enhanced (e.g., by capillarity) or a large elapsed time at elevated temperature is allowed [21]. This large diffusion-length effect may be significant even for small particles because of nonuniform mixing and agglomeration. Here, the nonuniform particle-size distribution is treated statistically and incorporated into the model.

The objective here is to develop a model capable of predicting the conversion to the final product and capturing the characteristics of the combustion front, i.e., the maximum temperature and the propagation speed. A temperature form of the energy equation is used with the goal of providing a direct comparison with simpler models (i.e., premixed-type combustion models). The model is developed for systems with a specimen-level stoichiometry rich in the low-melting temperature reactant and when the melting temperature of the high-melting temperature reactant is above the maximum temperature in the combustion zone. The extension to other stoichiometries requires additional considerations. The presentation is as broad as possible, but use is made of assumptions that simplify the mathematical treatment and allow for the analysis of the important physical and chemical mechanisms. The titanium–aluminum system is used as an example, but the model applicability is not restricted to this system.

In the following, an overview of the model is presented showing the connection between, the specimen-level and the particle-level treatments. Next, the specimen-level conservation equations and the thermodynamic considerations are presented. Then the particle-level model is presented, which incudes the interparticle-diffusion problem and the intraparticle-diffusion problem. The presentation begins with the interparticle-diffusion which depends on the particle-size distribution of the reactants and determines the amount of reactants available for chemical reaction. Then, the intraparticle-diffusion problem is presented which gives the reaction rates needed on the specimen-level model. Finally, the treatment of melting and solidification of the reactants and products is presented.

2. Model overview

At the specimen level, the medium is composed of particles of species A and B mixed at a specimen-level mass ratio. For $\langle \nu_A \rangle$ and $\langle \nu_B \rangle$ being the specimen-level number of moles of A and B, the global reaction leading to the equilibrium product C is (in a kmol of $C_{\langle \nu \rangle}$-basis)

[1] The term equilibrium model is used in a different context than that of the structural macrokinetics theory as reviewed by Merzhanov [2].

$$\langle v_A\rangle A+\langle v_B\rangle B \rightarrow C_{\langle v\rangle}. \quad (1)$$

Here species A and B are pure components, where A is a low-melting temperature metal, and $C_{\langle v\rangle}$ is the stoichiometric product with composition $\langle v_A\rangle$ atoms of A and $\langle v_B\rangle$ atoms of B.

For a nonequilibrium process, the conversion to $C_{\langle v\rangle}$ may not occur. At the particle level, it is assumed that the reaction between A and B forming C follows the relation (in a kmol of C-basis)

$$v_A A+v_B B \rightarrow C. \quad (2)$$

Figures 1 and 2 give an overview of the model. The model is based on a three-scales treatment, the specimen-level scale (specimen dimension L), the interparticle-level scale (interparticle diffusion characteristic length $l_D \sim l$), and the intraparticle-level scale (intraparticle diffusion characteristic length $l_d \sim R_B$). Figure 1 shows a rendering of the specimen-level and particle-level models. The specimen-level model (specimen-level scale) describes the local volume-averaged distributions of temperature and mass concentrations. The local volume averaging of a vector or scalar quantity ψ is defined by

$$\langle\psi\rangle = \frac{1}{V}\int_V \psi \, dV \quad (3)$$

where V is the volume of the local representative elementary volume (e.g., a unit cell) [Fig. 1(c)].

For a combustion front travelling from right to left, the local volume-averaged distributions of temperature and mass concentrations vary as rendered in Fig. 1(a). The dashed lines represent the distribution of temperature and mass concentrations for the adiabatic equilibrium case. The continuous lines correspond to the case where complete conversion is not achieved. Figure 1(c) presents a rendering of the unit cell. The unit cell is assumed to represent the average particle-level behavior and contains a representative number of all the particle sizes. This until cell is the local representative elementary volume of the specimen, over which the variables are volume averaged. The analysis requires that $l \ll l_F < L$ where L_F is the combustion zone thickness. In Fig. 1(c) it is shown the physical model with the melted reactant engulfing the solid reactant. Reaction occurs by intraparticle diffusion over the distance l_d. The distance separating the melt-rich regions to the melt-lean regions (distance l_D) is of the order of the unit cell characteristic length l. Figure 1(c) also shows the geometric model used for the treatment of the interparticle and the intraparticle diffusion. The intraparticle-diffusion model describes the evolution of the local concentration of the species along the radius of a single particle (represented as spherical). Figure 1(b) shows the transformations of the subunit cell as the combustion front travels along the specimen. Figure 2 shows the species distribution along the radius of the particle and the interfaces dividing the species A, B, and C domains. Figure 2(a) shows a conception of the intraparticle diffusion for slow diffusion conditions and Fig. 2(b) shows the nonequilibrium model used here. The phase diagram for the Al–Ti system and its relation to the particle-level model are also shown. Both Figs 1 and 2 will be discussed in more detail as the model is developed. In the following, the specimen-level model is discussed followed by the particle-level model.

3. Specimen-level model

3.1. Conservation equations

Here, it is assumed that the local thermal equilibrium exists between the phases. This assumption is based on the characteristics high thermal conductivity of metals. Therefore, although the local heat generation due to reaction and phase-change can be large and concentrated, the temperature gradients experienced at the unit cell level are assumed to be small when compared to the specimen-level temperature gradients. No movement of the liquid, gas, and solid phases is allowed. Some of the effects of liquid movement will be further discussed in connection with the interparticle diffusion model. The specimen-level transport equations are obtained from the volume averaging of the local point-wise conservation equations for mass, species, and energy. In the local volume-averaged conservation of species equation the specimen-level diffusion fluxes are neglected because diffusion of chemical species is expected to occur in the unit cell scale but not between unit cells. The point-wise energy equation is expressed in terms of enthalpy for the liquid and solid phases and then volume averaged. These volume-averaged energy equations are added, leading to a single equation for the local volume-averaged enthalpy. The enthalpies of the components are then related to temperature through the specific heat capacities and the heats of formation and phase change. A discussion of the thermal treatment of multiphase systems is given by Whitaker [23] and Kaviany [23, 24] and a derivation of the volume-averaged equations can be found in [35].

Assuming a quasi-steady propagation of the combustion front at a speed u_F, the conservation equations are transformed by the following coordinate transformation

$$x_1 = x+u_F t. \quad (4)$$

In the moving coordinate x_1, for a constant u_F, the conservation of species A becomes

$$\frac{d}{dx_1}u_F\langle\rho_A\rangle = \langle\dot{n}_{r,A}\rangle \quad (5)$$

where $\langle\dot{n}_{r,A}\rangle$ is the local volume-averaged homogeneous (volumetric) reaction rate of species A.

If the reaction is assumed to occur between liquid A and solid B, the equation for species A,l is

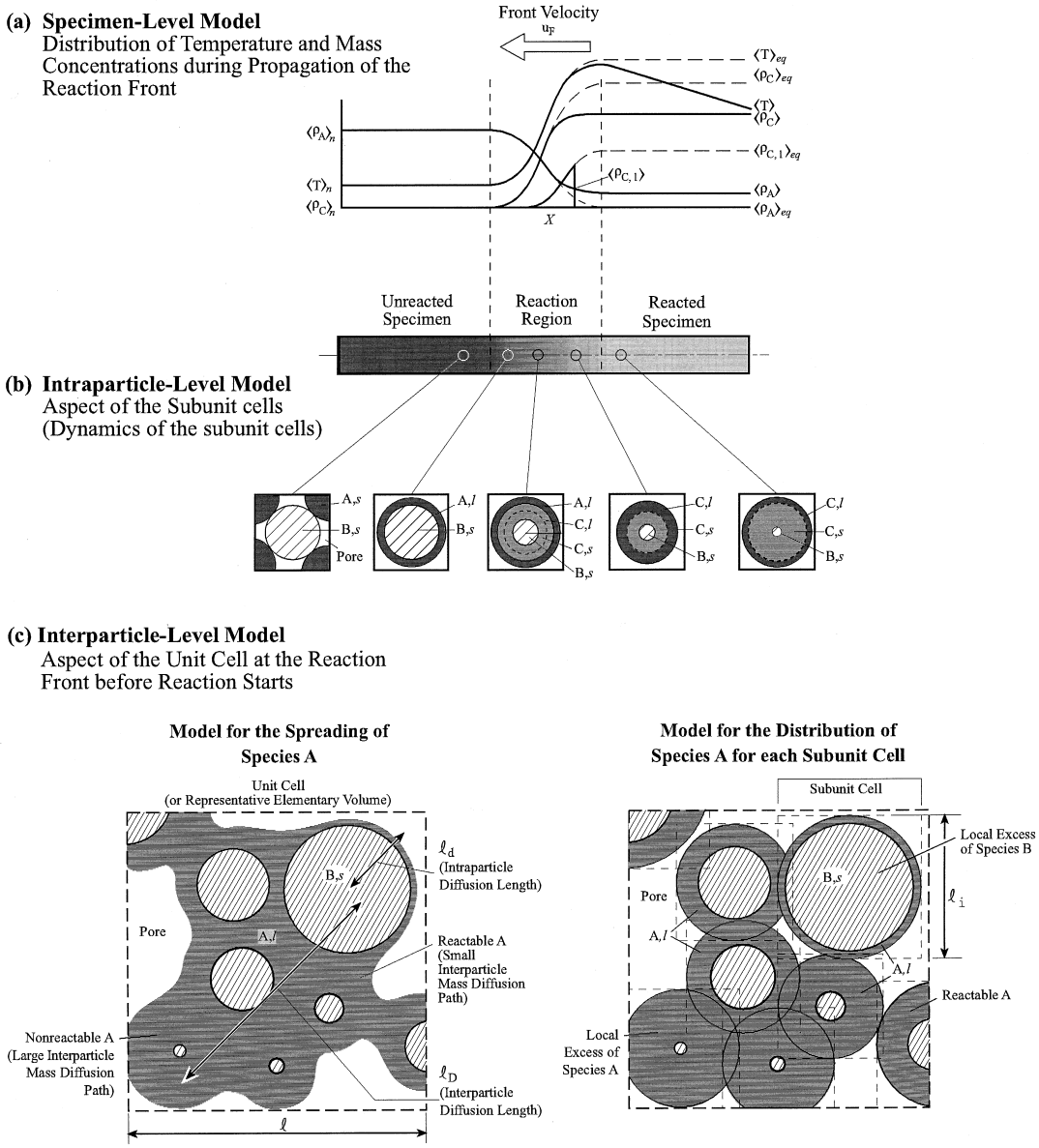

Fig. 1. (a) Rendering of the specimen-level temperature and mass concentration distributions, (b) variations in the structure of the subunit cell along the specimen, and (c) modeling of the nonuniform particle-size distribution, showing the subunit cells and the fraction of melted species A which may not reach the species B particles.

$$\frac{\mathrm{d}}{\mathrm{d}x_1}u_F\langle\rho_{A,l}\rangle = \langle\dot{n}_{r,A}\rangle + \langle\dot{n}_{ls,A}\rangle \tag{6}$$

where $\langle\dot{n}_{ls,A}\rangle$ is the volumetric melting rate of species A.

The consumption of species B and the production of species C are related to the consumption of A through their stoichiometric coefficients [equation (2)]. Assuming that C forms in the solid phase, the conservation of species C,l depends on the melting rate of C and is given by

$$\frac{\mathrm{d}}{\mathrm{d}x_1}u_F\langle\rho_{C,l}\rangle = \langle\dot{n}_{ls,C}\rangle. \tag{7}$$

The local volume-averaged energy equation is

$$\frac{\mathrm{d}}{\mathrm{d}x_1}\langle\rho\rangle c_p u_F\langle T\rangle = \frac{\mathrm{d}}{\mathrm{d}x_1}(\langle k\rangle + \langle k_r\rangle)\frac{\mathrm{d}\langle T\rangle}{\mathrm{d}x_1} + \Delta i_{r,A}\langle\dot{n}_{r,A}\rangle - \Delta i_{ls,A}\langle\dot{n}_{ls,A}\rangle - \Delta i_{ls,C}\langle\dot{n}_{ls,C}\rangle + \frac{A_{sa}h_{sa}}{V_s}(T_a - \langle T\rangle) \tag{8}$$

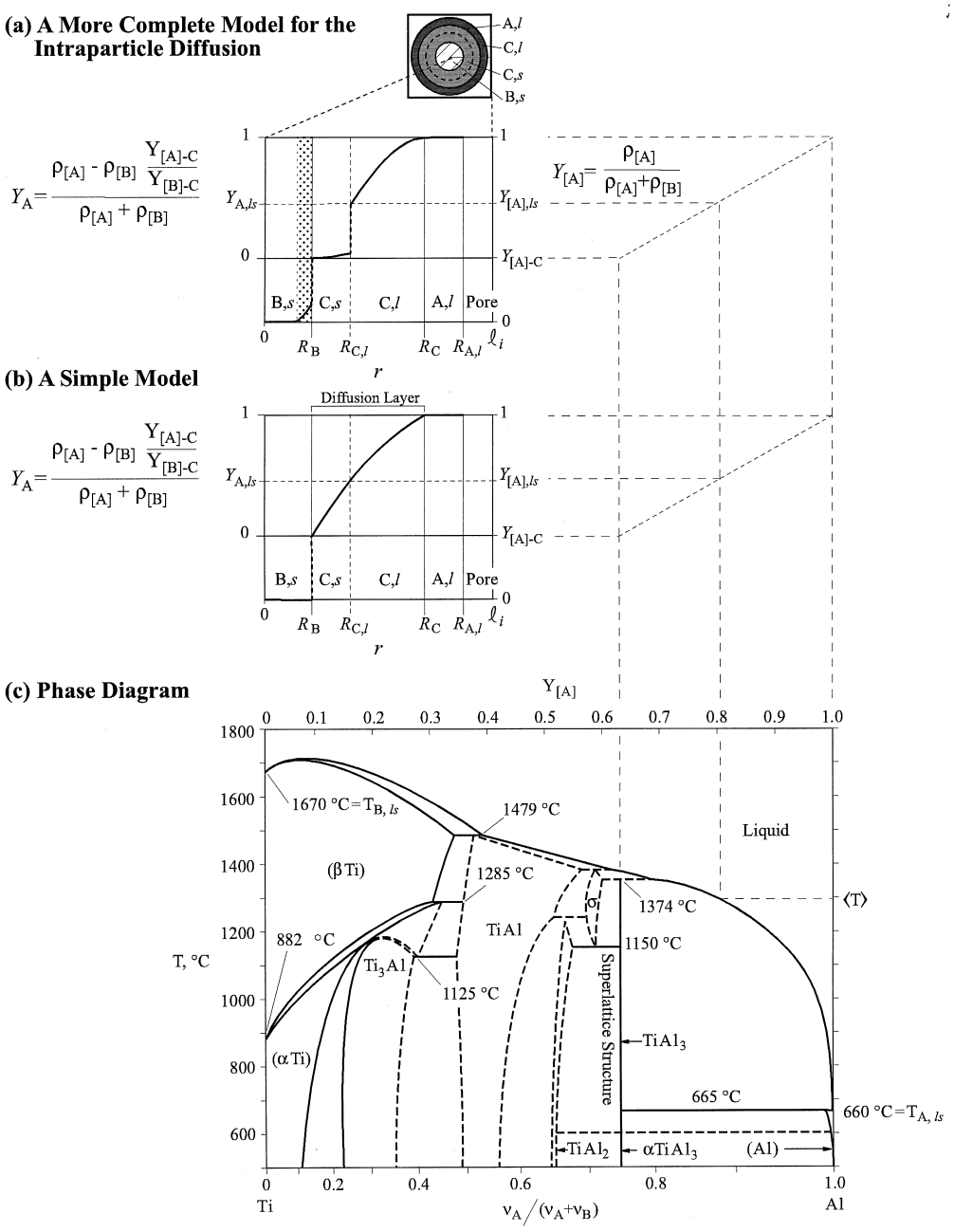

Fig. 2. Rendering of the particle-level species A mass fraction distribution for the subunit cell. (a) Conceptual model for the intraparticle diffusion, (b) the nonequilibrium intraparticle-diffusion model, and (c) the phase-diagram for the titanium–aluminum system.

where $\langle\rho\rangle c_p$ is the local volume-averaged volumetric heat capacity, $\langle k\rangle$ is the effective thermal conductivity, $\langle k_r\rangle$ is the effective radiant thermal conductivity, $\Delta i_{r,A}$ is the heat of reaction (on a mass of A-basis), $\Delta i_{ls,A}$ is the heat of melting of species A (on a mass of A-basis), $\Delta i_{ls,C}$ is the heat of melting of species C (on a mass C-basis), A_{sa} is the peripheral surface area of the specimen, h_{sa} is the average heat transfer coefficient between the specimen and the ambient, V_s is the local volume of the specimen, and T_a is the average ambient temperature.

The heat transfer from the specimen to the ambient (i.e., peripheral heat losses) has been modeled as a volu-

metric term and the average heat transfer coefficient includes the radiation heat transfer. For a cylindrical specimen, $A_{sa}/V_s = 4/D_s$.

The boundary and inial conditions for equations (5)–(8) are

$$x_1 \to -\infty, \langle\rho_A\rangle = \langle\rho_A\rangle_n, \langle\rho_B\rangle = \langle\rho_B\rangle_n, \langle\rho_C\rangle = \langle\rho_C\rangle_n, \langle T\rangle = \langle T\rangle_n, \langle\rho_{A,l}\rangle = \langle\rho_{C,l}\rangle = 0 \quad (9)$$

$$x_1 \to \infty, \frac{d\langle\rho_A\rangle}{dx_1} = \frac{d\langle T\rangle}{dx_1} = \frac{d\langle\rho_{A,l}\rangle}{dx_1} = \frac{d\langle\rho_{C,l}\rangle}{dx_1} = 0 \quad (10)$$

where the subscript n refers to the nonreacted condition (which is the same as the initial conditions).

The effective transport properties appearing in equation (8) (i.e., $\langle k\rangle$ and $\langle k_r\rangle$) need to be measured or estimated using approximate models [24].

The combustion front speed u_F is an eigenvalue of the problem and is obtained as part of the solution by the integration of the A-species equation, i.e.,

$$u_F = \frac{1}{\langle\rho_A\rangle_r - \langle\rho_A\rangle_n}\int_{-\infty}^{+\infty}\langle\dot{n}_{r,A}\rangle\,dx_1. \quad (11)$$

To complete the model, expressions are needed for the volume-averaged reaction rate and melting rates. These will be provided by the particle-level model. However, before presenting the particle-level model, it is necessary to obtain expressions for the heat of reaction $\Delta i_{r,A}$, heat of melting of C, $\Delta i_{ls,C}$, and the volume-averaged volumetric heat capacity $\langle\rho\rangle c_p$.

3.2. Thermodynamics

Here, the enthalpy of the condensed phases is a function of temperature only. We consider the formation of a single product C at the particle level and that $T_{ls,A} < T_{ls,C} < T_{ls,B}$. Also, we assume that the product C has a specific heat capacity equal to the average specific heat capacities of the reactants, i.e., $\Delta c_p = 0$ (Newman and Kopp's rule [25]); the species have the same (and constant) specific heat capacities in the liquid and solid phases ($c_{p,s} = c_{p,l}$); and species A and B are pure substances ($i_f^0 = 0$). The heat of reaction in a mass of A basis is then given by

$$\Delta i_{r,A} = \begin{cases} \dfrac{i_{f,C}^0}{Y_{A-C}} & \langle T\rangle < T_{ls,A} \\ \dfrac{i_{f,C}^0}{Y_{A-C}} - \Delta i_{ls,A} & T_{ls,A} \leqslant \langle T\rangle < T_{ls,C} \\ \dfrac{i_{f,C}^0}{Y_{A-C}} - \Delta i_{ls,A} + \dfrac{\Delta i_{ls,C}}{Y_{A-C}} & T_{ls,C} \leqslant \langle T\rangle < T_{ls,B} \\ \dfrac{i_{f,C}^0}{Y_{A-C}} - \Delta i_{ls,A} + \dfrac{\Delta i_{ls,C}}{Y_{A-C}} - \dfrac{Y_{B-C}}{Y_{A-C}}\Delta i_{ls,B} & \langle T\rangle \geqslant T_{ls,B} \end{cases} \quad (12)$$

where $Y_{A-C} = \nu_A M_A/(\nu_A M_A + \nu_B M_B)$ and $Y_{B-C} = 1 - Y_{A-C}$ are the mass fractions of species A and B in species C. For $T_{ls,A} < T_{ls,B} < T_{ls,C}$ the equations above are changed accordingly. Equation (12) can be extended if more than one product is present. The fact that the phase change temperatures have to be accounted for explicitly on the heat of reaction is the main disadvantage of the temperature form of the energy equation.

The heat of melting of species C is the difference between the enthalpy of the liquid solution of A and B and the enthalpy of the solid C at $T_{ls,C}$, i.e.,

$$\begin{aligned}\Delta i_{ls,C} &= i_{C,l}(T_{ls,C}) - i_{C,s}(T_{ls,C}) \\ &= Y_{A-C} i_A(T_{ls,C}) + Y_{B-C} i_B(T_{ls,C}) \\ &\quad + \Delta i_{m,C}(T_{ls,C}, Y_{A-C}, Y_{B-C}) - i_{C,s}(T_{ls,C}),\end{aligned} \quad (13)$$

where $\Delta i_{m,C}$ is the heat of mixing (heat of solution) of A and B at temperature $T_{ls,C}$ and compositions Y_{A-C} and Y_{B-C}.

Using the same simplifying assumptions listed above, $\Delta i_{ls,C}$ is given by

$$\Delta i_{ls,C} = -i_{f,C}^0 + Y_{A-C}\Delta i_{ls,A} + \Delta i_{m,A}. \quad (14)$$

The liquid solution of metals forming intermetallics is in general strongly nonideal [26]. If for lack of specific thermodynamic data we assume an ideal-solution behavior we have

$$\Delta i_{ls,C} = -i_{f,C}^0 + Y_{A-C}\Delta i_{ls,A}. \quad (15)$$

From the volume-averaged equations (5)–(8), and the equations for $\Delta i_{r,A}$ and $\Delta i_{ls,C}$, equations (12) and (15), we observe that there is no net heat generation for $T > T_{ls,C}$ when the heat of mixing is neglected.

The effective volumetric heat capacity is given by

$$\langle\rho\rangle c_p = \sum_{A,B,C}\langle\rho_i\rangle c_{p,i}. \quad (16)$$

Under the assumptions stated above, the effective specific heat capacity c_p is constant and calculated from

$$c_p = c_{p,C_{\langle v\rangle}} = Y_{A-C_{\langle v\rangle}} c_{p,A} + Y_{B-C_{\langle v\rangle}} c_{p,B}. \quad (17)$$

Also, $\langle\rho\rangle$ is constant and given by

$$\langle\rho\rangle = \langle\rho_A\rangle_n + \langle\rho_B\rangle_n + \langle\rho_C\rangle_n. \quad (18)$$

Later, $\langle\rho\rangle$ will be related with the initial porosity and composition of the specimen.

4. Particle-level model

In the following, first the effect of variable particle size (i.e., interparticle diffusion) is considered and then the intraparticle-diffusion model is discussed followed by the treatment of the melting of reactants and product.

4.1. Interparticle diffusion

Powders are characterized by a nonuniform distribution of particle size and shape. The size and shape of a single particle affect the diffusion and reaction through two mechanisms. First, the mass diffusion depends on the diffusion length and area characteristic of the particles. Second, the amount of heat generated for a given diffusion length depends on the volume associated with that diffusion length. Aris [27] showed that for steady-state, diffusion-controlled, first-order homogeneous reactions the reaction rate for arbitrarily shaped particles can be described as a function of a characteristic length equal to the ratio between the volume and the surface area. For the case of diffusion-controlled heterogeneous reactions there is no general shape factor (which can be easily shown for the quasi-steady approximation).

Therefore, in the absence of a general method, here the particles are modeled as ellipsoids with semiaxes $a_1 = R_{\max}$ and $a_2 = a_3 = R_{\min}$ (i.e., prolate spheroids) and the characteristic radius is given as the radius of the sphere with the same volume as the ellipsoid particle, i.e.,

$$R_i = (R_{\max,i} R_{\min,i}^2)^{1/3}. \tag{19}$$

The objective of using an ellipsoid is to approximate the volume of the powder particles because the total energy released by the chemical reaction, for complete reaction, is proportional to the volume of the particles. Therefore, the radius of the sphere with the equivalent volume satisfy the specimen-level equilibrium conditions.

The nonuniform particle size distribution has two effects. First, the volume-averaged reaction rate depends on the average of the reaction rates for each particle. Second, the nonuniform particle size results in non-stoichiometric distribution of reactants at the particle level. The distance separating the A-rich regions from the A-lean regions may be large and total product conversion may not be achieved. To treat the interparticle diffusion a statistical model, which incorporates the effect of the particle-size distribution of the high melting-temperature component, is developed. The model is developed for the case in which the resistance for the interparticle mass transfer is assumed large.

4.1.1. Variable particle size

From measurements, a particle size distribution function f_i [based on the radius given by equation (19)] is determined, where $f_i\Delta R$ is the number of particles with radius between $R_i - \Delta R/2$ and $R_i + \Delta R/2$ divided by the total number of particles in the sample. The particle size distribution (or number fraction) f_i is normalized, i.e., $\Sigma_{i=1}^{N} f_i \Delta R = 1$, where N is the number of bins in which the sample is divided (ΔR is the bin size).

The ensemble averaging of a quantity ψ_i is given by

$$\overline{\psi} = \sum_{i=1}^{N} \psi_i f_i \Delta R \tag{20}$$

and the total amount of a specific property ψ_i is,

$$\psi = N \sum_{i=1}^{N} \psi_i f_i \Delta R = N\overline{\psi}. \tag{21}$$

For instance, assuming that the reaction rate can be calculated for each species B particle (with initial radius $R_{B,i}$), the total reaction rate for the unit cell is

$$\dot{n}_r = N \sum_{i=1}^{N} \dot{n}_{r,i} f_i \Delta R = N\overline{\dot{n}_r}. \tag{22}$$

For the volume of the unit cell given by $V_l = N\overline{l^3}$, the volume-averaged reaction rate is

$$\langle \dot{n}_r \rangle = \frac{\overline{\dot{n}_r}}{\overline{l^3}}. \tag{23}$$

Similarly, if the mass of species A related to each species B particle is known, the volume averaged mass concentration of species A is,

$$\langle \rho_A \rangle = \frac{\overline{m_A}}{\overline{l^3}}. \tag{24}$$

These values of $\langle \dot{n}_r \rangle$ and $\langle \rho_A \rangle$ are the ones appearing in the specimen-level formulation. The major difficulty in applying equations (23) and (24) is the determination of $\overline{m_A}$. The nonuniform particle size distribution affects the packing and mixing of the powders and a subunit cell stoichiometry different from the specimen-level stoichiometry may exist. The solution for the packing problem is beyond the scope of this study. The approximation assumed here is that species A spreads over the surface of the B particles as a layer with the same mass, regardless of the B particle size. In order to satisfy the volume constraint given by equation (19), an average species B particle radius can be defined as the radius of the particle with the average volume, i.e.,

$$\overline{R_{B,n}^3} = \sum_{i=1}^{N} R_{B,i}^3 f_i \Delta R, \tag{25}$$

where $\overline{V_{B,n}} = 4\pi\overline{R_{B,n}^3}/3$.

For the specimen-level stoichiometry, the average mass of species A for each particle of species B, $m_{A,n}$, is given by

$$\overline{m_{A,n}} = \frac{Y_{A-\langle C \rangle}}{Y_{B-\langle C \rangle}} \rho_B^0 \overline{V_{B,n}}. \tag{26}$$

Given enough elapsed time at high temperatures, or by increasing the interparticle diffusion, the species A melt would migrate from the melt-rich to the melt-lean regions, causing a complete conversion. This is equivalent to a specimen-level equilibrium model. For large propagation speeds and under the presence of heat losses, this liquid migration may not be complete. For negligible liquid migration, the combustion would proceed under interparticle-level frozen conditions. It is likely that some

amount of interparticle liquid migration occurs in the time scale of the combustion synthesis of intermetallics. However, here we will assume that the resistance to melt movement is large, which corresponds to a lower limit for the conversion.

Neglecting the interparticle diffusion of species A, each species B particle can be treated as an isolated system and represented by a subunit cell, as depicted in Fig. 1(c). The subunit cells are assumed to have the same specimen level porosity ε_n. Note that strictly speaking this assumption would require a redistribution of the porosity around the particles thus altering the original packing existent in the unit cell. An alternative description would assume that the subunit cells are volumes surrounding each particle and fitting perfectly inside the unit cell. The first approach leads to simpler equations and is adopted here. The characteristic length of the subunit cells l_i is then given by

$$l_i^3 = \frac{4\pi}{3}\left(1+\frac{Y_{A-C,i,n}\rho_B^0}{Y_{B-C,i,n}\rho_A^0}\right)\frac{R_{B,i,n}^3}{1-\varepsilon_n} \tag{27}$$

where,

$$Y_{A-C,i,n} = \frac{m_{A,i,n}}{m_{A,i,n}+m_{B,i,n}}, \quad Y_{B-C,i,n} = 1 - Y_{A-C,i,n} \tag{28}$$

where $m_{A,i,n} = \overline{m_{A,n}}$ and $m_{B,i,n} = \rho_B^0 4\pi R_{B,i,n}^3/3$.

The initial local volume-averaged concentrations of species A and B for each subunit cell are

$$\langle\rho_A\rangle_{i,n} = \frac{m_{A,i,n}}{l_i^3}, \quad \langle\rho_B\rangle_{i,n} = \frac{m_{B,i,n}}{l_i^3} \tag{29}$$

and the total density, if the initial concentration of products is zero (no dilution with the final product), is $\langle\rho\rangle_{i,n} = \langle\rho_A\rangle_{i,n} + \langle\rho_B\rangle_{i,n}$.

From this initial mass of species A and from the initial radius of the species B particles, the reaction rates can be calculated (as it will be shown later). The conservation of mass equation [equations (5)] is applied for each subunit cell resulting in the local volume averaged concentrations of species A for each subunit cell. The specimen level local volume-averaged concentration of species A is then obtained from the ensemble averaging over all the subunit cells using equations (20) and (21). Analogously, the specimen level volume-averaged reaction rate is obtained from equation (20) and (21) and used in the specimen level energy equation [equation (8)]. This treatment is limited by the practical limits imposed on the number of subunit cells that can be used (number of bins used to represent the particle-size distribution function). Because of this, an average treatment of the conversion and reaction is desirable.

4.1.2. Average treatment

The assumption made is that the average intraparticle diffusion behavior of the unit cell can be approximated by the intraparticle diffusion behavior of the average species B particle. From the interparticle diffusion model the final conversion is determined a priori and the average mass of species A actually available for reaction is applied on the surface of the average species B particle. Thus, the equations for determination of the particle-level reaction rates are applied only to the average species B particle surrounded by the average species A shell available for conversion. This approach is adopted here because of its simplicity.

The determination of the average mass of species A available for reaction follows. Under the assumption of no interparticle metal migration, the species B particles with radius $R_{B,i} \leqslant \overline{R_{B,n}}$ are completely converted to product (because of the excess of species A) while those with $R_{b,i} > \overline{R_{B,n}}$ are only partially converted (because of the lack of species A). Thus, the fraction of species B completely converted (i.e., the volume of species B converted divided by the total inial volume of species B) is determined by

$$F_{B,c} = \frac{V_{B,c}}{V_B} = \frac{\sum_{i=1}^{N_1} f_i V_{B,i}\Delta R + \overline{V_{B,n}}\sum_{i=N_1}^{N} f_i\Delta R}{\sum_{i=1}^{N} f_i V_{B,i}\Delta R} = \sum_{i=1}^{N_1} f_i \frac{V_{B,i}}{\overline{V_{B,n}}}\Delta R + \sum_{i=N_1}^{N} f_i\Delta R \tag{30}$$

where $R_{B,i} < \overline{R_{B,n}}$ for $1 \leqslant i \leqslant N_1$, and $R_{B,i} > \overline{R_{B,n}}$ for $N_1 < i \leqslant N$.

This fraction approaches one as the distribution function becomes uniform (monosized particles) and zero as the spread (standard deviation) of the distribution function increases. From the average mass of species A, $\overline{m_{A,n}}$, the mass of A actually converted is $\overline{m_{A,c}} = F_{A,c}\overline{m_{A,n}}$, where $F_{A,c} = F_{B,c} = F_c$.

The characteristic length of the unit cell is given by

$$\overline{l^3} = \frac{4\pi}{3}\left(1+\frac{Y_{A-\langle C\rangle}}{Y_{B-\langle C\rangle}}\frac{\rho_B^0}{\rho_A^0}\right)\frac{\overline{R_{B,n}^3}}{1-\varepsilon_n}. \tag{31}$$

The local volume-averaged initial concentrations of species A and B are

$$\langle\rho_A\rangle_n = F_c\langle\rho_A\rangle_s, \quad \langle\rho_B\rangle_n = \langle\rho_B\rangle_s \tag{32}$$

where the average initial concentrations under stoichiometric conditions are

$$\langle\rho_A\rangle_s = \frac{\rho_A^0(1-\varepsilon_n)}{1+\frac{Y_{B-\langle C\rangle}}{Y_{A-\langle C\rangle}}\frac{\rho_A^0}{\rho_B^0}}, \quad \langle\rho_B\rangle_s = \frac{\rho_B^0(1-\varepsilon_n)}{1+\frac{Y_{A-\langle C\rangle}}{Y_{B-\langle C\rangle}}\frac{\rho_B^0}{\rho_A^0}}. \tag{33}$$

The determination of the particle-level reaction rate follows. This discussion applies equally for each particle $R_{B,i}$, or for the average particle $\overline{R_{B,n}}$.

4.2. Intraparticle diffusion

Here it is assumed that C has the same composition of $C_{\langle v\rangle}$. This assumption is in general valid when the

specimen-level stoichiometry is rich in the low melting temperature species A [29, 30].

Figure 2 shows the various radii used to identify the concentric spherical shell layers. The mass fraction of elements A and B are $Y_{[A]}=\rho_{[A]}/(\rho_{[A]}+\rho_{[B]})$ and $Y_{[B]}=\rho_{[B]}/(\rho_{[A]}+\rho_{[B]})$ while the mass fractions of species A and C are

$$Y_A=\frac{\rho_{[A]}-\dfrac{Y_{[A]-C}}{Y_{[B]-C}}\rho_{[B]}}{\rho_{[A]}+\rho_{[B]}},\quad Y_C=\frac{\left(1+\dfrac{Y_{[A]-C}}{Y_{[B]-C}}\right)\rho_{[B]}}{\rho_{[A]}+\rho_{[B]}} \tag{34}$$

where $Y_{[A]-C}=v_AM_A/(v_AM_A+v_BM_B)$ and $Y_{[B]-C}=1-Y_{[A]-C}$.

Here, a simplified treatment of the intraparticle diffusion is developed, leading to closed-form solutions for the reaction and melting rates. Figure 2(a) shows a rendering of the intraparticle diffusion. The extent of the solid intermetallic layer C, s depends on the type and kinetics of nucleation of the solid phase from a saturated liquid solution of A and B atoms. There may be formation of a solid layer covering the B particles (for heterogeneous nucleation) or there may be precipitation of solid grains in the solid solution (homogeneous nucleation). The solubility of species A on the solid intermetallic C, s may be small and the species B may present a solubility range for species A, variable with temperature. In the absence of interfacial barriers, the interfaces are under local phase equilibrium and at the interface between the A-rich intermetallic C and particle B other intermetallic phases may nucleate when the conditions are appropriate [this is the shaded region in Fig. 2(a)]. Here, a simplified model is developed, as shown in Figure 2(b). Regarding the product formation, this treatment assumes that species C is formed through the diffusion-controlled heterogeneous reaction of species A and B at the surface of the species B particle. Regarding the diffusion process, species A and C are assumed to diffuse through the diffusion layer (A–C layer). The solubility of species A on species B is assumed negligible. Species C solid is assumed to have an appreciable solubility of species A and its interface with the liquid phase is not in phase equilibrium. The concentration of species A on the outside surface of the diffusion layer depends on the presence of species A. The melting of species C is dictated by diffusion and energy requirements. The A–C mixture is assumed liquid for concentrations of species A exceeding the liquids line concentration $Y_{A,ls}$ at temperature $\langle T\rangle$, and solid for smaller concentrations.

Even this simplified model is complicated by the moving boundary, the spatially variable density (along the diffusion layer), the difference between diffusion coefficients for liquid and solid phases, and the time variation of the volume-averaged temperature (which affects the diffusion coefficient). In the search for a simple mathematical model, the following approximations are made: (1) for the Al–Ti system assuming that $TiAl_3$ is formed at the interface, the velocity of the R_B interface dR_B/dt is about 36% of the diffusion velocity of the A atoms at the interface $V_{[A]}$ (this can be obtained from a mass balance of species B and from the stoichiometry of the reaction). The velocity of the R_C interface is proportional to $(R_B/R_C)^2$. When $R_C=R_B$, $dR_C/dT=V_A$ and it drops to 25% of $V_{[A]}$ when $R_C=2R_B$. Therefore for most of the regime of interest, the boundary velocities are a fraction of the diffusion velocity. Here, the effect of the boundary movement on the solution of the diffusion equation is neglected (it is incorporated later when the particle-level model is coupled with the specimen-level model). This assumption becomes worse as the molecular weight of species B increases. (2) The relation between the mass fluxes of species A and C at the interface R_B is $\dot m_C|_{R_B}=-\dot m_A|_{R_B}(\rho_B^0-Y_{[B]-C}\rho_C^0)/Y_{[A]-C}\rho_B^0$. Assuming that C is an ideal solution of A and B, $\dot m_C|_{R_B}=-\dot m_A|_{R_B}\phi_A/Y_{[A]-C}$, where ϕ_A is the volume fraction of A. For $TiAl_3$, $\dot m_C|_{R_B}=-1.17\dot m_A|_{R_B}$. With the ideal solution hypothesis we have $dR_A/dt=0$ and $\dot m_C|_{R_A}=-\dot m_A|_{R_A}$. For simplicity, we then assume that species A and C counter-diffuse and the convective velocity u is therefore zero. (3) The density of the diffusion layer varies from ρ_C^0, at R_B, to ρ_A^0, at R_A, which corresponds to a 17% variation. Therefore, as a first approximation the density of the diffusion layer ρ is assumed constant. Note that later this effect will be also incorporated in the model. (4) Finally, the diffusion coefficient is assumed constant with time. Later it will, however, be calculated as a function of the volume-averaged temperature. It is important to observe that the solution of the complete problem for the closed, multi-shell, spherical system, with moving boundaries, spatially variable density, and time(temperature)-dependent diffusion coefficient requires a numerical solution for the intraparticle diffusion. This leads to additional computational time and, possible, a small effect on the overall conclusions. As there are many uncertainties about the nature of the products formed (solid or liquid phase) and the mechanisms of product formation (growth of a solid layer precipitation from a saturated liquid solution) there is very little justification for the development of a mathematically complex model. The assumptions adopted here lead to mathematically simple, first-order solutions which capture the most important aspects of the phenomenon.

Therefore, based on the simplifications above, for a frame of reference centered on the B particle (which is assumed static) the diffusion of species A in the A–C layer is given by

$$\frac{\partial Y_A}{\partial t}=\frac{1}{r^2}\frac{\partial}{\partial r}r^2D_{A-C}\frac{\partial Y_A}{\partial r} \tag{35}$$

with following initial and boundary conditions

$$t=0,\quad R_C=R_B+\Delta R_B,\quad Y_A=0 \tag{36}$$

$$t > 0, \quad r = R_C, \quad Y_A = Y_A|_{R_c} \tag{37}$$

$$t > 0, \quad r = R_B, \quad Y_A = 0. \tag{38}$$

For $t = 0$, in order to avoid a singularity, it is assumed that the B particles are covered by a small layer ΔR_B of product. The diffusion coefficient $D_{A\text{–}C}$ is assumed to be an average value for the solid and liquid product layer and it is modeled as an Arrhenius-type relation [28], i.e.,

$$D_{A—C} = D_0 \exp\left(\frac{-\Delta E_{a,D}}{R_g\langle T\rangle}\right) \tag{39}$$

where D_0 is a diffusion pre-exponential factor, $\Delta E_{a,D}$ is a diffusion activation energy, and R_g is the universal gas constant. Here, it is assumed that both the pre-exponential factor and the activation energy for the interdiffusion coefficient are constant with concentration.

The value of Y_A at R_C depends on the extent of the diffusion of species A. We define a primary-diffusion regime as the regime (space on the moving coordinate x_1) where there is species A available outside the diffusion layer. The secondary-diffusion regime is defined as the regime where there is no species A available outside the diffusion layer and the concentration of species A at R_C diminishes monotonically with respect to time. The boundary condition stated by equation (37) is then restated as

Primary-diffusion regime

$$Y_A|_{R_C} = 1 \tag{40}$$

Secondary-diffusion regime

$$\left.\frac{\partial Y_A}{\partial r}\right|_{R_C} = 0. \tag{41}$$

The solution for the primary and secondary regimes is discussed below.

4.2.1. Primary-diffusion regime

From the discussion above on the diffusion velocity, for the primary-diffusion regime a quasi-steady solution is adopted. Equation (35) then becomes

$$\frac{d}{dr} r^2 \frac{dY_A}{dr} = 0 \tag{42}$$

with the boundary conditions given by equation (40) and (38).

The solution to equation (42) is

$$Y_A = \frac{R_C}{r}\left(\frac{r - R_B}{R_C - R_B}\right). \tag{43}$$

The local reaction rate is

$$\dot{n}_{r,A} = -4\pi R_B^2 \rho D_{A\text{–}C} \left.\frac{\partial Y_A}{\partial r}\right|_{R_B} \tag{44}$$

where ρ is the average density of the diffusion layer. Later this average density will be calculated based on the specimen-level species concentration.

From equation (43),

$$\dot{n}_{r,A} = -4\pi \frac{R_B R_C}{R_C - R_B} \rho D_{A\text{–}C}. \tag{45}$$

From equation (23), the local volume-averaged reaction rate is then given by

$$\langle \dot{n}_{r,A}\rangle = -\frac{4\pi}{l^3} \frac{R_B R_C}{R_C - R_B} \rho D_{A\text{–}C} \tag{46}$$

where l^3 is either the volume of the subunit cell or the average volume of the unit-cell.

Note that equation (46) is a function of $\langle T\rangle$, through the diffusion coefficient, and of the local volume-averaged concentration of the reactants and products, which determine R_B and R_C. Later the radii R_B and R_C will be related to the local volume-averaged concentrations of B and C.

4.2.2. Secondary-diffusion regime

In the secondary-diffusion regime, a simple solution for equation (35) subjected to the boundary conditions given by equations (41) and (38) is obtained using a first-order Kantorovich integral method. The solution is assumed as a product of space and time-dependent functions. The space-dependent function is assumed to be parabolic and the coefficients are determined from the boundary conditions. The diffusion equation is integrated between R_B and R_C and the convective flux due to the movement of the interface at R_C is neglected (when compared to the diffusion flux). The final equation is obtained matching the mass of species A, as predicted for the beginning of the secondary-diffusion regime, with the mass of species A predicted at the end of the primary-diffusion regime. This gives

$$Y_A = \frac{3}{\pi}\frac{m_{A,D}}{\rho} \frac{(r - R_B)(R_C^2 - R_B r)}{r^2 (R_C - R_B)^2 (4R_C^3 - R_B R_C^2 - 2R_B^2 R_C - R_B^3)}. \tag{47}$$

From equation (23), the local volume-averaged reaction rate is

$$\langle \dot{n}_{r,A}\rangle = -\frac{12}{l^3} \frac{R_B(R_C + R_B)}{(R_C - R_B)^2 (4R_C^2 + 3R_C R_B + R_B^2)} m_{A,D} D_{A\text{–}C}. \tag{48}$$

In the secondary-diffusion regime all the species A is inside the diffusion layer. So, from equation (35) we can express $m_{A,D}$ as

$$m_{A,D} = l^3 \langle \rho_A\rangle. \tag{49}$$

Therefore, equation (48) can be restated as

$$\langle \dot{n}_{r,A}\rangle = -12 \frac{R_B(R_C + R_B)}{(R_C - R_B)^2 (4R_C^2 + 3R_C R_B + R_B^2)} \langle \rho_A\rangle D_{A\text{–}C}. \tag{50}$$

Equations (46) and (50) could be interpreted as, respectively, a zeroth-order and a first-order reaction kinetics if the terms containing the radii could be assumed

constant for some conditions. However, in general the various radii that define the unit cell are functions of the local volume-averaged concentrations and change along x_1, as it is shown next.

4.2.3. Coupling of particle- and specimen-level models

From the local volume-averaged concentrations of A, B and C, for any instant of time (or distance along x_1) R_B and R_C are determined from

$$R_B = \left(\frac{3}{4\pi}\frac{l^3\langle\rho_B\rangle}{\rho_B^0}\right)^{1/3}, \quad R_C = \left(R_B^3 + \frac{3}{4\pi}\frac{l^3\langle\rho_C\rangle}{\langle\rho_C\rangle^{A-C}}\right)^{1/3} \tag{51}$$

where $\langle\rho_C\rangle^{A-C}$ is the local volume-averaged density of component C in the A–C (diffusion) layer.

To identify the transition from the primary- to the secondary-diffusion regime the mass of species A available outside the diffusion layer $m_{A,F}$ is monitored. For the primary-diffusion regime the total mass of species A present in the unit cell, m_A, is determined from

$$m_A = l^3\langle\rho_A\rangle = m_{A,D} + m_{A,F}. \tag{52}$$

The mass of species A diffused during the primary-diffusion regime is determined by integration of equation (43), i.e.,

$$m_{A,D} = \tfrac{2}{3}\pi\rho R_C(2R_C^2 - R_C R_B - R_B^2). \tag{53}$$

Then, $m_{A,F}$ is determined from equation (52). The primary-diffusion regime ends when there is no species A available outside the diffusion layer.

The local volume-averaged density of the diffusion layer $\rho \equiv \langle\rho\rangle^{A-C}$ is determined from

$$\rho \equiv \langle\rho\rangle^{A-C} = \frac{1}{\dfrac{\langle Y_C\rangle^{A-C}}{\rho_C^0} + \dfrac{\langle Y_A\rangle^{A-C}}{\rho_A^0}}, \tag{54}$$

where $\langle Y_i\rangle^{A-C}$ is the local volume-averaged mass fraction of component i in the A–C (diffusion) layer. $\langle Y_A\rangle^{A-C}$ and $\langle Y_C\rangle^{A-C}$ are determined from the mass of species A and C inside the diffusion layer, if R_B and R_C, are known. R_B and R_C are calculated from equation (51), where R_C is a function of $\langle\rho\rangle^{A-C}$ through

$$\langle\rho_C\rangle^{A-C} = \langle Y_C\rangle^{A-C}\langle\rho\rangle^{A-C}. \tag{55}$$

Therefore, through an iterative procedure, both $\langle\rho\rangle^{A-C}$ and the geometry of the unit cell can be determined as a function of $\langle\rho_A\rangle$, for a given stoichiometry and initial particle size.

4.3. Phase change

Melting of species A is assumed to occur at $\langle T\rangle = T_{A,ls}$. Assuming that enough energy is generated from the chemical reaction (that is one of the requirements for propagation), the melting rate of the species A is given by

$$\langle\dot{n}_{A,ls}\rangle = -u_F\frac{\langle\rho_A\rangle}{\Delta x_1} \tag{56}$$

where Δx_1 is the size of the control-volume where the melting takes place. In the limit of $\Delta x_1 \to 0$, the melting of species A takes place at the interface between the liquid and solid phases, instead of volumetrically. For this limit, the energy equation requires a jump condition, between the liquid and solid phase domains.

The phase change of the product C is modeled as a diffusion-controlled regime followed by an energy-controlled regime. At a given time (or a location on the transformed coordinate), the temperature of the unit cell is $\langle T\rangle$ and the mass concentration of species A, $\langle\rho_A\rangle$, determines the Y_A distribution within the diffusion layer [either given by equation (43) or equation (47)]. From $\langle T\rangle$, the atomic concentration of species A on the liquidus line $Y_{[A],ls}$ is determined from the phase diagram and $Y_{A,ls}$ is obtained from equation (34). In the diffusion-controlled regime, it is assumed that the product layer is in the liquid state when $Y_A > Y_{A,ls}$ and in the solid state otherwise. The position of the interface between the solid and the liquid products is determined from equation (43) and (47), by setting $Y_{A,ls} = Y_A$. This gives

Primary-diffusion regime

$$R_{C,l} = \frac{R_C R_B}{Y_{A,ls}R_B + (1 - Y_{A,ls})R_C} \tag{57}$$

Secondary-diffusion regime

$$\left(\frac{R_{C,l}}{R_C}\right)^2 - \left[\frac{2Y_{A,ls}}{Y_A|_{R_C}} + \left(\frac{R_B}{R_C} + \frac{R_C}{R_B}\right)\left(1 - \frac{Y_{A,ls}}{Y_A|_{R_C}}\right)\right]\left(\frac{R_{C,l}}{R_C}\right) + 1 = 0 \tag{58}$$

where $Y_A|_{R_C}$ is the local mass fraction of species A at r_C as determined from equation (43) or (47) and equation (58) is valid for $Y_A|_{R_C} > Y_{A,ls}$. From a mass balance of species C between R_C and $R_{C,l}$, the mass of C,l, $m_{C,l}$ is given by

Primary-diffusion regime

$$m_{C,l} = \frac{2}{3}\pi\rho\frac{R_C^3 + 2R_{C,l}^3 - 3R_C R_{C,l}}{R_C - R_B} \tag{59}$$

Secondary-diffusion regime

$$m_{C,l} = \frac{4\pi\rho}{3}(R_C^3 - R_{C,l}^3) - m_{A,d} \times \left[\frac{3R_B(R_C^4 - R_{C,l}^4) - 4(R_C^2 + R_B^2) \times (R_C^3 - R_{C,l}^3) + 6R_B R_C^2(R_C^2 - R_{C,l}^2)}{(R_B - R_C)^2(R_B^3 + 2R_C R_B^2 + R_C^2 R_B - 4R_C^3)}\right]. \tag{60}$$

Finally, the product melting rate is obtained from

$$\langle \dot{n}_{\mathrm{C,ls}} \rangle = \frac{u_{\mathrm{F}}}{l^3} \frac{\mathrm{d}m_{\mathrm{C,l}}}{\mathrm{d}x_1}. \tag{61}$$

A similar procedure [equations (56) and (61)], but under strict equilibrium conditions, is used by Nekrasov et al. [17] and Smolyakov et al. [18] to obtain the product melting rate.

When $Y_{\mathrm{A}}|_{R_{\mathrm{C}}} \leqslant Y_{A,ls}$, the product layer behaves as a pure substance. In this case, the phase change becomes energy controlled. For the energy-controlled regime, two possible solidification paths are possible. If enough energy is generated by the reaction, the local volume-averaged temperature would follow the liquidus line temperature, and the amount of liquid is obtained from the energy equation and the species conservation equations rearranged as

$$\begin{aligned}
&\Delta i_{\mathrm{ls,C}} u_{\mathrm{F}} \frac{\mathrm{d}\langle \rho_{\mathrm{C,l}} \rangle}{\mathrm{d}x_1} \\
&\quad = -\frac{\mathrm{d}}{\mathrm{d}x_1}\left[\langle \rho \rangle c_{\mathrm{p}} u_{\mathrm{F}} \langle T \rangle - (\langle k \rangle + \langle k_{\mathrm{r}} \rangle) \frac{\mathrm{d}\langle T \rangle}{\mathrm{d}x_1} \right] \\
&\quad + \Delta i_{\mathrm{r,A}} u_{\mathrm{F}} \frac{\mathrm{d}\langle \rho_{\mathrm{A}} \rangle}{\mathrm{d}x_1} - \Delta i_{\mathrm{ls,A}} u_{\mathrm{F}} \frac{\mathrm{d}\langle \rho_{\mathrm{A,l}} \rangle}{\mathrm{d}x_1} \\
&\quad + \frac{A_{\mathrm{sa}} h_{\mathrm{sa}}}{V_{\mathrm{s}}} (T_{\mathrm{a}} - \langle T \rangle).
\end{aligned} \tag{62}$$

In the case when not enough energy is available, the solidification would happen instantly where $\langle T \rangle = T_{\mathrm{ls}}$ and the solidification rate is given by

$$\langle \dot{n}_{\mathrm{C,ls}} \rangle = -u_{\mathrm{F}} \frac{\langle \rho_{\mathrm{C,l}} \rangle}{\Delta x_1}. \tag{63}$$

The first case (equation (62)) occurs for large rates of interparticle diffusion or uniform particle-size distribution.

5. Conclusions

A three-scale, particle/level/specimen-level treatment is applied to the gasless compacted-powder combustion synthesis. The specimen-level treatment is based on the local volume-averaged equations for species and energy. The particle-level treatment assumes that the product is formed through a diffusion-controlled heterogeneous reaction at the surface of the high melting temperature reactant. The interparticle diffusion is modeled with two regimes: an initial primary-diffusion regime followed by a slower secondary-diffusion regime. The availability of reactants depends on the interparticle diffusion from the melt-rich regions to the melt-lean regions and this transport is influenced by the particle-size distribution.

The nonuniform particle-size distribution has two effects. Initially, since the chemical reaction is diffusion controlled, particles of different sizes experience different reaction rates and temperature evolution, thus, influencing the specimen-level temperature distribution and propagation speed. The average reaction rate can then be calculated from the ensemble averaging of the reaction rates for each particle size, or approximated by the reaction rate of a particle with the average size. The second effect is related to the local availability of the reactants. A heterogeneous distribution of reactants changes the local stoichiometry and the distance separating the melt-rich regions from the melt-lean regions [distance l_{D} in Fig. 2(a)] may be large. The peripheral heat losses, would then prevent the timely migration of the melted reactant. Here we have assumed a large resistance for interparticle mass transfer and, as a result, the final conversion is determined a priori.

This possible lack of complete conversion has a strong effect on the maximum temperature and the propagation speed. During the time scale characteristic of the combustion of intermetallics some liquid migration is expected to occur. The modeling of this interparticle diffusion requires descriptions of the spatial distribution of melt-rich and melt-lean regions, the transport mechanism (potential and transport coefficients), and the path for the transport. Both the potential and the transport coefficient may be strongly temperature dependent. These aspects of the interparticle-diffusion are not treated here. We plan to include the finite interparticle diffusion as a follow up. The combined effect of the secondary-diffusion regime and the interparticle-diffusion would extend the thickness of the reaction region and may explain the 'burn-out' phenomena reported in the literature [12].

Melting of the product follows the phase-equilibrium conditions and is characterized by a diffusion-controlled regime followed by an energy-controlled regime. The melting or solidification of products is an additional mechanism for redistribution of heat in the combustion zone, thus affecting the propagation speed and maximum temperature.

Another aspect not treated here involves the formation of intermediate compounds. The conversion to the final product may be preceded by the formation of intermediate compounds, depending on the system and on the specimen-level stoichiometry (Kachelmeyer [21]), e.g., when specimen-level stoichiometries rich in the high-melting temperature component are used. The formation of compounds at the interface between two phases depends on the thermodynamic equilibrium conditions and on the kinetics of nucleation and growth of the new phase. There are in turn affected by the atomic diffusion at the interface (Hoyt and Brush [31], Ma et al. [32]) making it possible the formation of metastable phases and the equilibrium product may not be formed during the time-scale of the combustion front propagation. The formation of intermediate compounds was not addressed here. The model developed by Hodaj and Desré [33] based on the critical gradient concept $(\nabla c)_{\mathrm{c}}$ could be possibly used to model the product formation.

In a follow-up article (Part II, Oliveira and Kaviany [34]) this model will be applied to the titanium–aluminum system with specimen-level composition corresponding to $TiAl_3$.

Acknowledgements

The financial support of the Conselho Nacional de Desenvolvimento Científico e Tecnológico-CNPq, Brazil, and the US National Science Foundation are appreciated.

References

[1] Z.A. Munir, Synthesis of high temperature materials by self-propagating combustion methods, Ceramic Bulletin 67 (1988) 342–349.
[2] A.G. Merzhanov, Self-propagating high-temperature synthesis: twenty years of search and findings, in: Z.A. Munir, J.B. Holt (Eds.), Combustion and Plasma Synthesis of High Temperature Materials, Chap. 1. VCH Publishers, New York, 1990.
[3] A. Varma, J.-P. Lebrat, Combustions synthesis of advanced materials, Chem. Eng. Sci. 47 (1992) 2179–2193.
[4] H.G. Kaper, G.K. Leaf, S.B. Margolis, B.J. Matkowski, On nonadiabatic condensed phase combustion, Combust. Sci. Tech. 53 (1987) 289–314.
[5] A. Varma, G. Cao, M. Morbidelli, Self-propagating solid–solid noncatalytic reactions in finite pellets, AIChE Journal 36 (1990) 1032–1038.
[6] M.G. Lakshmikhanta, J.A. Sekhar, An investigation of the effect of porosity and diluents on micropyretic synthesis, Metallurgical Transactions A 24A (1993) 617–628.
[7] H.J. Viljoen, J.A. Puszynski, Analysis of propagation characteristics during nonadiabatic condensed phase combustion, Journal of Materials Synthesis and Processing 2 (1994) 247–253.
[8] A.P. Aldushin, T.M. Martem'yanova, A.G. Merzhanov, B.I. Khaikin, K.G. Shkadinskii, Propagation of the front of an exothermic reaction in condensed mixtures with the interaction of the components through a layer of high-melting product, Comb. Exp. Shock Waves 8 (1972) 159–167.
[9] S.D. Dunmead, Z. Munir, Temperature profile analysis in combustion synthesis: I. Theory and background, J. Am. Ceramic. Soc. 75 (1992) 175–179.
[10] A.P. Hardt, P.V. Phung, Propagation of gasless reactions in solids—I. Analytical study of exothermic intermetallic reaction rates, Combust. Flame 21 (1973) 77–89.
[11] R. Armstrong, Models for gasless combustion in layered materials and random media, Combust. Sci. Tech. 71 (1990) 155–174.
[12] R. Armstrong, Theoretical models for the combustion of alloyable materials, Metallurgical Transactions A 23A (1992) 2339–2347.
[13] A. Makino, C.K. Law, Heterogeneous flame propagating in the self-propagating high-temperature synthesis (SHS) process: theory and experimental comparison, Proceedings of the Twenty-Fourth International Symposium on Combustion, The Combustion Institute, Pittsburg, 1992, pp. 1883–1891.
[14] A. Makino, C.K. Law, SHS combustion characteristics of several ceramic and intermetallic compounds, J. Am. Ceram. Soc. 77 (1994) 778–786.
[15] Y. Zhang, G.C., Stangle, A micromechanistic model of the combustion synthesis process: II. Numerical simulation, J. Mater. Res. 9 (1994) 2605–2619.
[16] A.P. Aldushin, B.I. Khaikin, Combustion of mixtures forming condensed reaction products, Comb. Exp. Shock Waves 10 (1974) 273–280.
[17] E.A. Nekrasov, V.K. Smolyakov, Y.M. Maksimov, Mathematical model for the titanium–carbon system combustion, Comb. Exp. Shock Waves 17 (1981) 513–520.
[18] V.K. Smoliakov, E.A. Nekrasov, Y.M. Maksimov, Modeling gas-free combustion with phase transitions, Comb. Exp. Shock Waves 20 (1992) 182–191.
[19] A. Makino, C.K. Law, Bimodal particle dispersion in the nonadiabatic heterogeneous SHS flame propagation, Comb. Sci. and Tech. 106 (1995) 193–201.
[20] A.P. Aldushin, B.I. Khaikin, K.G. Shkadinsky, Effect of the inhomogeneity of the internal structure of the medium on the combustion of condensed mixtures, interacting through a layer of product, Comb. Exp. Shock Waves 12 (1976) 725–731.
[21] C.R. Kachelmyer, J.-P, Lebrat, A. Varma, P.J. McGinn, Combustion synthesis of intermetallic aluminides: processing and mechanistic studies, in: B. Farouk, M. Pinar Menguc, R. Viskanta, C. Presser, S. Chellaiah (Eds.), Heat Transfer in Fire and Combustion Systems, ASME HTD-Vol. 250, New York, 1993, pp. 271–276.
[22] M. Kaviany, Principles of Heat Transfer in Porous Media, 2nd edn., Springer-Verlag, New York, 1995.
[23] S. Whitaker, Simultaneous heat, mass, and momentum transfer in a porous media: a theory of drying, in: J.P. Harttnet, I. Irvine (Eds.), Advances in Heat Transfer, Academic Press, New York, 1977, pp. 119–203.
[24] M. Kaviany, Principles of Convective Heat Transfer, Springer-Verlag, New York, 1994.
[25] O. Kubaschewski, C.B. Alcock, P.J. Spencer, Materials Thermochemistry, 6th ed., Pergamon Press, Oxford, 1993.
[26] D.R. Gaskell, Introduction to Metallurgical Thermodynamics, 2nd ed., Taylor and Francis, New York, 1981.
[27] R. Aris, On shape factors for irregular particles—I. The steady-state problem. Diffusion and reaction, Chem. Engng Sci. 6 (1957) 262–268.
[28] L.N. Larikov, Diffusion, in: J.H. Westbrook, R.L. Fleischer (Eds.), Intermetallic Compounds, Vol. 1, Principles, Wiley, New York, 1994, pp. 757–770.
[29] R. de Reus, Diffusion barriers, in: J.H. Westbrook, R.L. Fleischer (Eds.), Intermetallic Compounds, Vol. 2, Practice, Wiley, New York, 1994, pp. 603–635.
[30] D.E., Alman, J.A. Hawk, A.V. Petty, Jr., J.C. Rawers, Processing intermetallic composites by self-propagating high-temperature combustion synthesis, Journal of Metals (1994) 31–35.
[31] J.J. Hoyt, L.N. Brush, On the nucleation of an intermediate phase at an interface in the presence of a concentration gradient, J. Appl. Phys. 78 (1995) 1589–1594.

[32] E. Ma, C.V. Thompson, L.A. Clevenger, Nucleation and growth during reactions in multilayer Al/Ni films: the early stage of Al_3Ni formation, J. Appl. Phys 69 (1991) 2211–2218.

[33] F. Hodaj, P.J. Desré, Effect of a sharp gradient of concentration on nucleation of intermetallics at interfaces between polycrystaline layers, Acta Materialia 44 (1996) 4485–4490.

[34] A.A.M. Oliveira, M. Kaviany, Role of inter- and intra-particle diffusion in nonuniform particle size gasless compacted-powder combustion synthesis—II: results and comparison with experiment. Int. J. Heat Mass Transfer 42 (1999) 1075–1095.

[35] A.A.M. Oliveira, Effect of particle-level and specimen-level transport on product state in compacted-powder combustion synthesis and thermal debinding of polymers from molded powders. Ph.D. Thesis, The University of Michigan, Ann Arbor, MI, 1998.